Title
Top—down versus bottom—up oxidation of a neonicotinoid pesticide by OH radicals

Journal
Proceedings of the National Academy of Sciences of the United States of America, 121(7)

ISSN
0027-8424

Authors
Wang, Xinke
Wang, Weihong
Wingen, Lisa M
et al.

Publication Date
2024-02-13

DOI
10.1073/pnas.2312930121

Peer reviewed

PNAS RESEARCH ARTICLE | ENVIRONMENTAL SCIENCES OPEN ACCESS

Top–down versus bottom–up oxidation of a neonicotinoid pesticide by OH radicals

Xinke Wang[a,1], Weihong Wang[a,1], Lisa M. Wingen[a], Véronique Perraud[a], and Barbara J. Finlayson-Pitts[a,2]

Edited by Vicki H. Grassian, University of California, San Diego, La Jolla, CA; received July 27, 2023; accepted November 17, 2023 by Editorial Board Member Akkihebbal R. Ravishankara

Emerging contaminants (EC) distributed on surfaces in the environment can be oxidized by gas phase species (top–down) or by oxidants generated by the underlying substrate (bottom–up). One class of EC is the neonicotinoid (NN) pesticides that are widely distributed in air, water, and on plant and soil surfaces as well as on airborne dust and building materials. This study investigates the OH oxidation of the systemic NN pesticide acetamiprid (ACM) at room temperature. ACM on particles and as thin films on solid substrates were oxidized by OH radicals either from the gas phase or from an underlying TiO_2 or $NaNO_2$ substrate, and for comparison, in the aqueous phase. The site of OH attack is both the secondary $>CH_2$ group as well as the primary $-CH_3$ group attached to the tertiary amine nitrogen, with the latter dominating. In the case of top–down oxidation of ACM by gas phase OH radicals, addition to the –CN group also occurs. Major products are carbonyls and alcohols, but in the presence of sufficient water, their hydrolyzed products dominate. Kinetics measurements show ACM is more reactive toward gas phase OH radicals than other NN nitroguanidines, with an atmospheric lifetime of a few days. Bottom–up oxidation of ACM on TiO_2 exposed to sunlight outdoors (temperatures were above 30 °C) was also shown to occur and is likely to be competitive with top–down oxidation. These findings highlight the different potential oxidation processes for EC and provide key data for assessing their environmental fates and toxicologies.

emerging contaminants | acetamiprid | OH radical | nitrite | TiO_2

Significance

Emerging contaminants (EC) are widely dispersed in the environment and undergo various degradation processes, potentially changing their environmental fates and impacts. This study demonstrates that the products and mechanisms of the OH oxidation of the neonicotinoid acetamiprid are determined by whether OH attacks from the gas phase (top–down), the underlying substrate (bottom–up), or in the aqueous phase. An important result is that the bottom–up oxidation of acetamiprid on TiO_2, which is widely present in airborne particles, building exteriors, etc., is an important degradation pathway. This comprehensive knowledge of oxidation pathways will inform strategies to mitigate the impacts of EC on the environment and human health.

Heterocyclic nitrogen-containing compounds and complex amines are commonly found in various synthetic substances that have become widely distributed in the environment. These emerging contaminants (EC) include pesticides and pharmaceuticals as well as materials used in consumer products and in munitions. An example of such compounds is the neonicotinoid (NN) pesticides, which were developed in the early 1990 s and which have become the most widely used pesticides globally where they are applied as seed coatings and to soils and as foliar sprays (1, 2). NNs have been detected in runoff into rivers and lakes, as well as in soil, dust particles, wildflowers, pollen, nectar, and honey (2–7). Not surprisingly, they are also detected in food (8, 9), drinking water (10), and human blood and urine (11, 12). The increasing use and widespread distribution of NNs have been accompanied by deleterious environmental impacts particularly on pollinators such as honeybees, which have experienced significant declines and bee colony collapse over the last several decades (13–18).

Therefore, significant attention has been devoted to investigating the degradation of such EC in water and soils (2, 19–24) both because of their presence in surface waters and for purposes of removing them from wastewater. However, characterization of their interactions with atmospheric oxidants remains scarce. The atmospheric oxidation of EC can occur through the interaction with gas phase species such as the hydroxyl radical (OH), which we refer to as "top–down" chemistry. A much less studied possibility is oxidation from the "bottom–up" by oxidants generated photochemically by the substrates themselves (25). Such is the case for titanium dioxide (TiO_2) and nitrate and nitrite ions which are widely distributed in soils, airborne particles, and building materials. This area of oxidation reactions of EC on aerosol particles and solid substrates remains relatively unexplored, including for the NN pesticides used as an example in the present study.

The NNs are systemic pesticides that are distributed throughout the plant as well as on other surfaces such as soil, airborne particles, and building surfaces. Another circumstance in which NNs can be found on surfaces is when they are dissolved in water which contains salts, metal oxides, and organics. Drying of such multi-component aqueous mixtures leads to an increase in the concentration of the salt component, triggering phase separation through the salting-out of the organic component and ultimately resulting in the formation of distinct structures such as core-shell or partially engulfed configurations (26, 27). Such liquid–liquid phase separation often plays an important role in the aerosol chemistry that

Author affiliations: [a]Department of Chemistry, University of California, Irvine, CA 92697-2025

Author contributions: B.J.F.-P. designed the research; X.W., W.W., L.M.W., and V.P. performed research; X.W. and W.W. analyzed data; and X.W., W.W., and B.J.F.-P. wrote the paper.

The authors declare no competing interest.

This article is a PNAS Direct Submission. V.H.G. is a guest editor invited by the Editorial Board.

[1]X.W. and W.W. contributed equally to this work.

[2]To whom correspondence may be addressed. Email: bjfinlay@uci.edu.

This article contains supporting information online at https://www.pnas.org/lookup/suppl/doi:10.1073/pnas.2312930121/-/DCSupplemental.

Published February 5, 2024.

occurs in the atmosphere (28–31). While the top–down and bottom–up pathways may have distinct oxidation mechanisms and products, little is known about the differences between the two modes of attack. The lack of such oxidation reaction studies of EC may result in a biased assessment of their ecological and health impacts.

Acetamiprid (ACM) is one of the most widely used NNs and extensive research efforts have been devoted to investigating the kinetics and products of ACM oxidation in the aqueous phase, including wastewater (32–40). However, to date, the oxidation reactions of solid films of ACM on aerosol particles by gas phase species and by those generated by solid substrates remain unexplored. This study bridges this critical research gap by providing a comprehensive examination of ACM oxidation through a dual top–down and bottom–up approach as shown in Fig. 1. Elucidating the fate and behavior of ACM across diverse situations that are found in the environment is more broadly applicable to other EC as well and provides key data for assessing their environmental fates.

Results and Discussion

Table 1 summarizes the products and relative amounts observed under all conditions of the bottom–up and top–down studies reported here and for comparison those in aqueous phase OH oxidation experiments. The structures of these products were determined either through MS/MS analysis (*SI Appendix*, Fig. S1) using Orbitrap HRMS or by comparison with the retention times and MS/MS spectra of authentic standards. For convenience in discussing these products and their mechanisms of formation, we have assigned abbreviated names to each one as shown in Table 1. To facilitate discussion of the mechanisms, we use the following carbon numbering system:

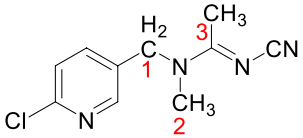

Acetamiprid (ACM)

Aqueous Phase OH Oxidation of ACM. For comparison to the literature and to the $NaNO_2$ bottom–up experiments, the oxidation of ACM in aqueous solution was studied, where OH was generated by the photolysis of nitrite. As seen in Fig. 2, the major product observed was ACM-desm (*m/z* 209), with a molar yield of 0.23 ± 0.02 (1σ) defined as Δ product/Δ ACM (only a trace amount was seen in the control experiment with NaCl substituted for $NaNO_2$). Quantification of ACM-desm and 6-chloronicotinic acid (CNA, *m/z* 158) was carried out using authentic standards. Indirect calibrations for Carbonyl-A, Carbonyl-B and Alcohol-A were developed based on their hydrolysis to form ACM-desm and CNA (Fig. 3 and *SI Appendix*, Fig. S2 and *Text S1*). There was also significant mass spectral peak intensity at *m/z* 98 (ACM-P1) in which scission of the aromatic ring from the parent ACM has occurred. However, this product could not be quantified due to the lack of an authentic standard. Small amounts of CNA were also detected. These products are consistent with previous reports (32, 38, 40) where H_2O_2 or O_3 were used as OH sources.

Fig. 4 shows the proposed mechanism of formation of the observed products. The highlighted pathways show the formation of ACM-desm and ACM-P1 based on well-known OH-organic chemistry in the presence of O_2 and NO (41) and do not involve water. The two carbonyl compounds A and B (*m/z* 237) and alcohols A and B (*m/z* 239) can also be formed in parallel pathways via RO_2 + RO_2 reactions, in addition to RO_2 + NO. These were major products for experiments in the absence of water as discussed below, but as a result of the hydrolysis of Carbonyl-A, Carbonyl-B and Alcohol-A (Fig. 3), only small peaks due to these products are observed in the aqueous OH-ACM oxidation, while that for the hydrolysis product ACM-desm is large.

Hydrogen abstraction by OH can occur at the secondary carbon (C1) or at a primary carbon (C2 or C3). For simple hydrocarbons, attack at the secondary >CH_2 group is normally much faster than at a primary -CH_3 group, typically by about a factor of seven (42). However, the products observed here and indeed in all of our experiments, suggest that hydrogen abstraction at the primary carbon (C2) dominates over that at the secondary carbon (C1). In the case of the aqueous phase oxidation, ACM-desm is formed both from the direct oxidation (Fig. 4) as well as from the hydrolysis of Carbonyl-A and Alcohol-A (Fig. 3), which arise from hydrogen abstraction from C2. No products from hydrogen abstraction at C3 were observed.

The relatively high reactivity of a primary –CH_3 group was also observed in the OH reactions with NN dinotefuran (DNF) and clothianidin (CLD) (43). This effect was attributed to a much lower bond dissociation energy (BDE) difference of 4 kJ mol^{-1} between primary and secondary C–H groups that are adjacent to an amine nitrogen (44, 45). For primary vs. secondary C–H

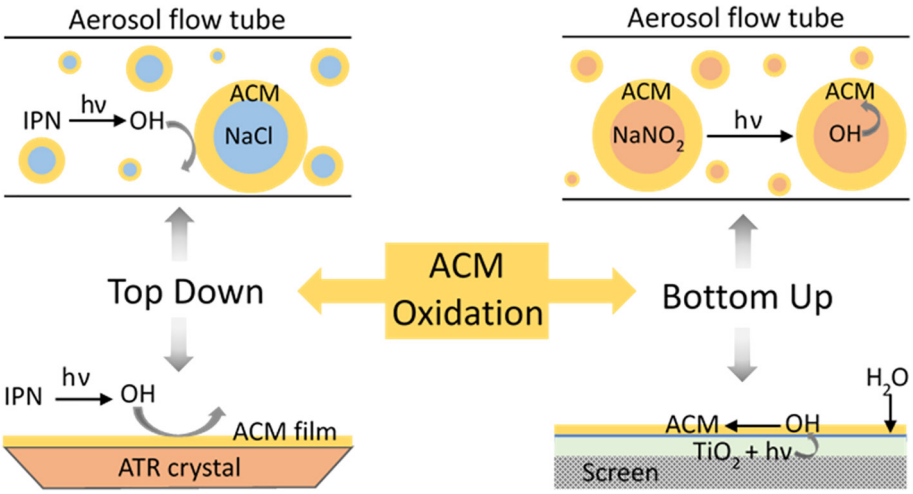

Fig. 1. Schematics of OH oxidation systems for acetamiprid from the top–down and bottom–up in both particles and thin solid films.

Table 1. Products and relative amounts observed under all conditions of the bottom–up and top–down oxidations as well as those in aqueous phase OH oxidation experiments*

Compound† (MW)	Abbreviated name and observed *m/z*	Error (ppm)	Aqueous	Bottom–up: Thin film on TiO_2 RH 50%	Bottom–up: On $NaNO_2$ particles§ RH 22 to 27%	Top–down with IPN: On NaCl particles RH 6 to 8%	Top–down with IPN: On NaCl particles RH 33 to 37%	Top–down with IPN: Thin film on ATR RH 0%	Top–down with IPN: Thin film on ATR RH 50%
Acetamiprid (MW 222.7)	ACM 223.0742	−1.3							
(E)-*N*-((6-chloropyridin-3-yl) methyl)-*N′*-cyano-*N*-formylacetimidamide (MW 236.7)	Carbonyl-A 237.0535	−1.3	S	L	—	L	L	L	L
(E)-6-chloro-*N*-(1-(cyanoimino) ethyl)- *N*-methylnicotinamide (MW 236.7)	Carbonyl-B 237.0535	−1.3	S	M	—	L	L	M	M
N-(6-Chloro-3-pyridylmethyl)-*N′*-cyano-acetamidine (MW 208.7)	ACM-desm 209.0590	0.5	L	M	L	M	M	M	M
(E)-*N′*-Cyano-*N*-methylethanimidamide (MW 97.1)	ACM-P1 98.0713	0.0	M	M	S	S	S	M	M
6-chloronicotinaldehyde (MW 141.6)	ACM-P2‡ 142.0056	1.4	S	—	—	S	S	S	S
6-chloronicotinic acid (MW 157.6)	CNA 158.0001	−1.3	S	S	M	S	S	—	—
(E)-*N*-((6-chloropyridin-3-yl) methyl)-*N′*-cyano-*N*-(hydroxymethyl)-acetimidamide (MW 238.7)	Alcohol-A 239.0691	−1.3	S	S	—	S	S	L	L
(E)-*N*-((6-chloropyridin-3-yl) (hydroxy) methyl)-*N′*-cyano-*N*-methylacetimidamide (MW 238.7)	Alcohol-B 239.0691	−1.3	S	—	—	S	S	—	—
N-((6-chloropyridin-3-yl) methyl)-*N*- methylacetimid-amide (MW 197.7)	ACM-descn 198.0797	2.0	—	—	—	L	M	L	S
(E)-*N′*-Carbamoyl-*N*-((6-chloropyridin-3-yl) methyl)-*N*-methylacetimidamide (MW 240.7)	ACM-P3 241.0847	−1.7	—	—	—	S	S	S	S
(E)-*N*-((6-chloropyridin-3-yl) methyl)-*N*-methyl-*N′*-nitroacetimidamide (MW 242.7)	ACM-P4 243.0818	−0.8	—	—	—	S	S	M	S

*Relative amounts of product formation are denoted as follows: L, large; M, medium; S, small; and "—", not detected.
†See Figs. 3, 4, and 9 for structures.
‡Only measured by UHPLC-Orbitrap MS.
§After subtracting out reaction on NaCl particles.

groups in simple alkanes this difference is much larger, ~13 kJ mol^{-1} (41), which drives the attack at the secondary C–H bonds.

Bottom–Up OH Oxidation of ACM. A number of species found in the condensed phase in the Earth system are photocatalysts that generate OH radicals upon irradiation. These include TiO_2 found as a solid and nitrite or nitrate salts found as solids or in aqueous droplets. TiO_2 is a photocatalyst and present in the Earth's crust at 0.44% (w:w) and in dust particles at locations around the world (41, 46). In addition, TiO_2 has been widely applied in building exteriors, floor tiles, road pavements, and windows (46–50). The photolysis of TiO_2 generates OH radicals at the interface via the formation of electron–hole pairs that react with water (46, 51–54) (*Materials and Methods*). This is a well-known photocatalytic oxidation process used for water treatment (23, 37, 55, 56) and also presents a potential oxidation mechanism on soil, atmospheric dust particles, and building surfaces containing this oxide (46, 57, 58).

Similarly, nitrite is widely distributed in natural waters (59, 60), soils (61, 62), and the atmosphere (63). Although nitrite is typically found in the environment at low concentrations, its high molar absorptivity and photolysis quantum yield (64) can render it a significant photoreactant under environmental conditions (59). Nitrite anions photolyze to generate O^- which reacts with water to form OH radicals (*Materials and Methods*).

Hence, studies were carried out using TiO_2 and $NaNO_2$ as OH sources for oxidation from the bottom–up at 22 °C. As shown in Fig. 5 *A* and *B*, particles of NaCl or $NaNO_2$ coated with ACM clearly exhibit organic–inorganic phase separation. ACM (formula, $C_{10}H_{11}N_4Cl$) indicated by nitrogen or chlorine, forms a shell around the NaCl or $NaNO_2$ cores. For all experiments, the relative humidity (RH) was below the deliquescence points for both $NaNO_2$ (67%) (65) and NaCl (75%) (66) to maintain phase separation. *SI Appendix*, Fig. S3 shows that in the ACM and TiO_2 film experiment, the TiO_2 surface was also coated by ACM, providing a second platform for investigating bottom–up oxidation

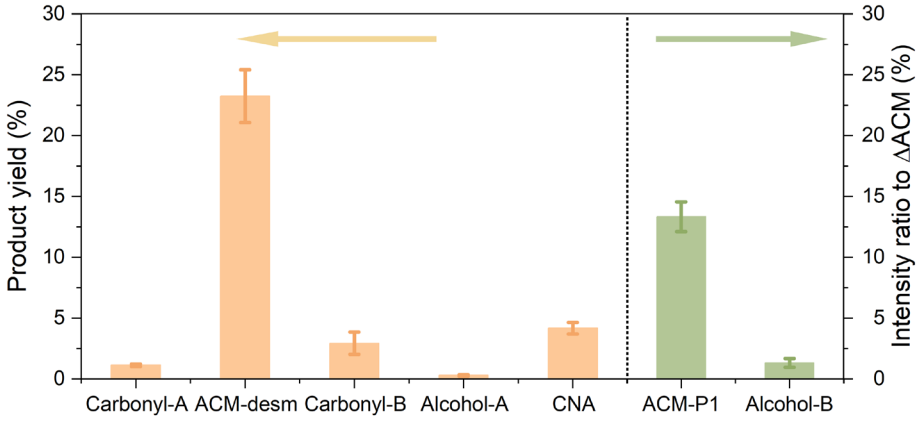

Fig. 2. Product yields (*Left* axis) and intensity ratios to the loss of ACM, ΔACM, (*Right* axis) in the aqueous phase oxidation of ACM after 18 h of irradiation.

processes. The ACM film is likely to be amorphous due to its formation from fast evaporation of the solvent and its lower tendency to crystallize (67, 68).

TiO_2 substrate. Fig. 6 shows the products obtained from photolysis of ACM-coated TiO_2 deposited onto a screen (Fig. 1) at 50% RH in air. The primary product observed was Carbonyl-A, followed by smaller yields of ACM-desm and Carbonyl-B. Much smaller amounts of Alcohol-A and CNA were measured, and ACM-P1 was also identified but not quantified. Since there was no source of NO in this system, the RO_2 + RO_2 channel (Fig. 4) must provide the reaction pathway. The RO_2 + RO_2 reaction has a number of pathways, forming a carbonyl + alcohol, 2 RO, or peroxides (ROOR) (69). The first pathway would give equal amounts of the carbonyl and alcohol products, whereas the second one would lead to the carbonyl products. The higher yield of Carbonyl-A relative to Alcohol-A (Fig. 6) suggests that the 2 RO pathway dominates. The higher yield of Carbonyl-A relative to Carbonyl-B shows that abstraction of hydrogen is again favored from the $–CH_3$ group (C2) on the nitrogen (Fig. 4).

All of the identified products were those expected based on the well-established principles of OH-organic reactions. Thus, while a small contribution from the direct reaction between ACM and excited TiO_2, or its associated holes/electrons, cannot be definitively ruled out, there is no evidence for this from our experiments. For example, products from the bottom–up oxidation by two different substrates, TiO_2 and $NaNO_2$, are both consistent with OH oxidation when hydrolysis of the carbonyl products and alcohol-A are taken into account.

The different product distributions for ACM-coated TiO_2 compared to the aqueous OH-oxidation provide some insight into the mechanisms. Thus, in water, the carbonyl and alcohol products hydrolyze to form ACM-desm, the major product observed. In the case of TiO_2 at 50% RH, there is surface-adsorbed water which is sufficient to generate OH but not enough to hydrolyze the carbonyl products that are formed. The accessibility of the TiO_2 surface to water vapor depends on whether the ACM coating completely covers the TiO_2. TEM-EDS images of the sample (*SI Appendix*, Fig. S3) show that the nitrogen is colocated with the titanium, suggesting that ACM is relatively evenly spread on the oxide on a macro/micron scale. However, the fact that oxidation does indeed occur indicates that there are areas on a molecular scale that are accessible for water vapor to reach the TiO_2 surface. For comparison, studies (23, 35) of ACM oxidation in aqueous solution with a slurry of TiO_2 reported ACM-desm as the major product, similar to that in aqueous solutions observed here and in earlier studies (32, 38, 40). The aqueous environment clearly favors hydrolysis of the initially formed carbonyl and alcohol products, but this is not the case for TiO_2 with surface-adsorbed water. Thus, in dust particles and soils as well as building surfaces containing TiO_2, carbonyls are expected as major products from this bottom–up oxidation.

$NaNO_2$ substrate. The bottom–up oxidation of acetamiprid used ACM-coated $NaNO_2$ particles suspended in air in the aerosol flow tube (AFT, Fig. 1 and *SI Appendix*, Fig. S4*A*). ACM-coated NaCl particles were used as a control. Absolute product yields

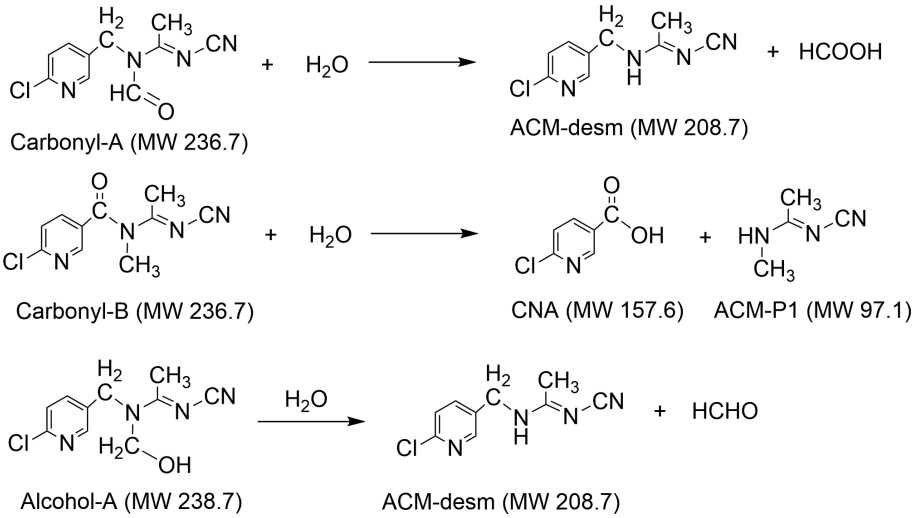

Fig. 3. Hydrolysis of ACM carbonyl- and alcohol-products.

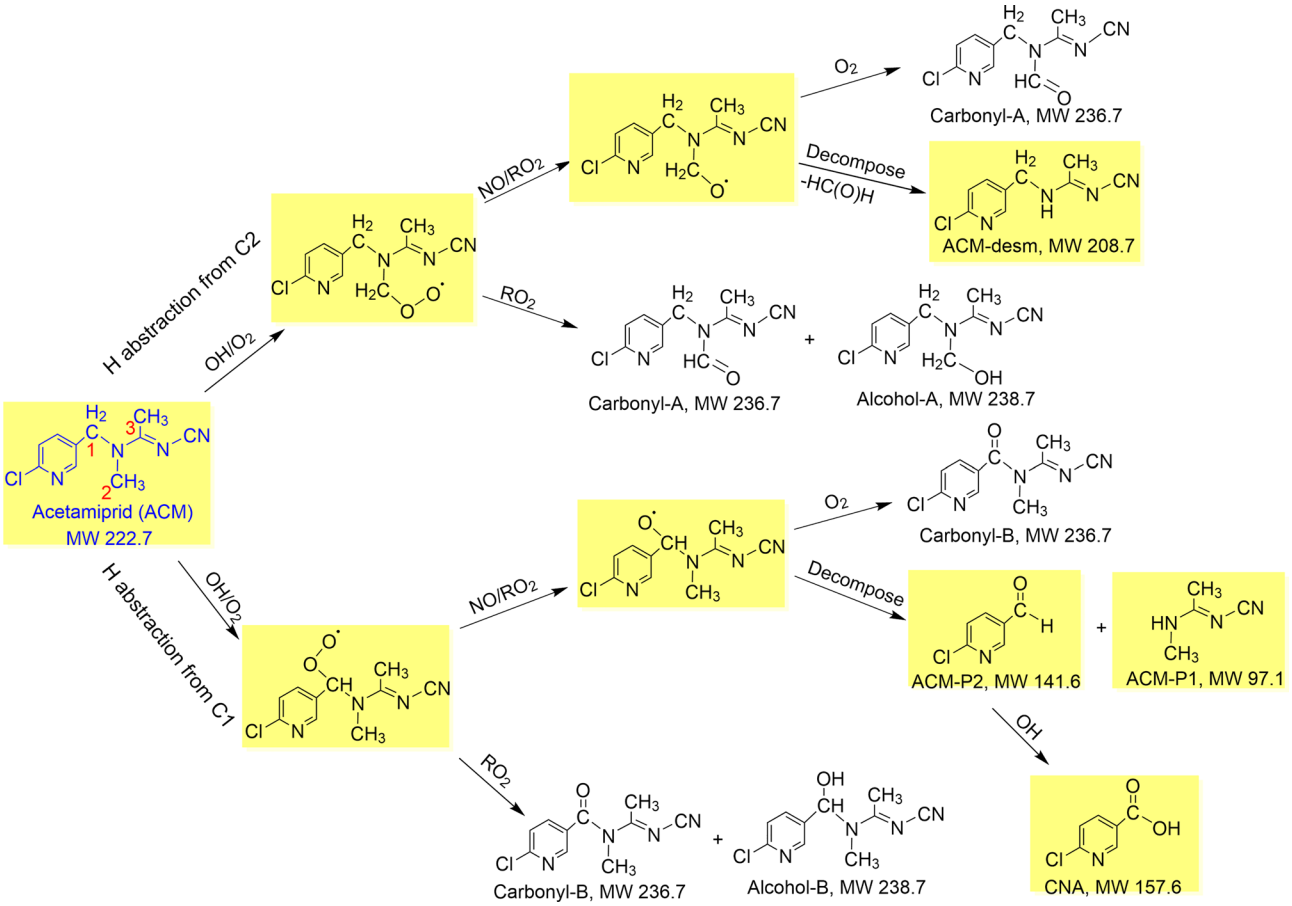

Fig. 4. Proposed mechanisms for the formation of the major products from the ACM + OH reaction. The highlighted pathways show the formation of ACM-desm and ACM-P1 based on well-known OH-organic chemistry in the presence of O_2 and NO.

could not be measured for AFT experiments due to small total loss of ACM and variations in the mass loading on the filters. However, molar ratios relative to the unreacted ACM remaining in the samples after reaction could be obtained. Fig. 7*A* shows the molar ratio of products to the unreacted ACM formed in the photolysis of ACM + $NaNO_2$ and ACM + NaCl particles at RH 22 to 27%. ACM-desm is the major product, with CNA and ACM-P1 formed in significant yields as well. Small amounts of Carbonyl-A, Carbonyl-B and Alcohol-A were detected in both $NaNO_2$ and NaCl experiments with a similar molar ratio to unreacted ACM, suggesting that they were mainly formed from direct photolysis in the organic shell as a result of some light absorption in the 300 to 350 nm range (*SI Appendix*, Fig. S5). Fig. 7*B* shows ACM-desm, CNA, and ACM-P1 increase with RH. This reflects that increasing water increases OH production via reaction of O^- from the NO_2^- photolysis with H_2O and also increases the hydrolysis of Carbonyl-A, Carbonyl-B and Alcohol-A to form these products (Fig. 3).

Even under dry conditions (<5% RH), there were some OH oxidation products observed. $NaNO_2$ is known to be hygroscopic (70), and during the drying process, some water may remain when phase separation occurs. To further assess the presence of residual water in the particles after the silica dryer, a custom-designed impactor was utilized for collecting the particles on a ZnSe ATR crystal (71). The FTIR spectra (*SI Appendix*, Fig. S6) show a broad water peak around 3,200 to 3,600 cm^{-1}. After purging the FTIR sample compartment until the RH decreased to ~4%, adsorbed water bands were still observed, indicating the persistence of water within the particle core or adsorbed on the particle surface. Thus, OH production and the oxidation of ACM may continue at quite low relative humidity.

Top–Down OH Oxidation of ACM. The investigation of top–down oxidation of ACM was conducted using the photolysis of isopropyl nitrite (IPN) as the gas phase OH source at 22 °C. Two types of ACM samples were used: 1) ACM-coated NaCl particles in air exposed to OH radicals in a flow tube and collected on filters (Fig. 1 and *SI Appendix*, Fig. S4*A*) and 2) a thin film of ACM either on a screen followed by extraction into a solvent, or on an ATR crystal where the loss of ACM and formation of products could be followed in real time (Fig. 1 and *SI Appendix*, Fig. S4 *B* and *C*). Due to the absence of water, hydrolysis of products as identified in the aqueous reactions and bottom–up oxidations does not occur, and the full suite of products in Table 1 is observed in the UHPLC-HESI(+)-Orbitrap MS extracted ion chromatograms (EICs) from particles collected on filters from the flow tube (*SI Appendix*, Figs. S7 and S8 and *Text S2*). No products were detected under dark conditions with IPN. In the absence of IPN but under irradiation, several ACM photolysis products were detected in small amounts relative to that in the presence of IPN (*SI Appendix*, Fig. S9).

Absolute product yields also could not be measured for ACM-NaCl particles, but molar ratios relative to the unreacted ACM in the samples are shown in Fig. 8*A*. Also shown are the relative peak intensities for products that could not be quantified (Fig. 8*B*). Carbonyl-A and Carbonyl-B are major products, with smaller amounts of ACM-desm, Alcohol-A, and CNA. Increasing the RH from 6 to 8% to 33 to 37% did not impact their molar ratios significantly, indicating that relatively little water that would

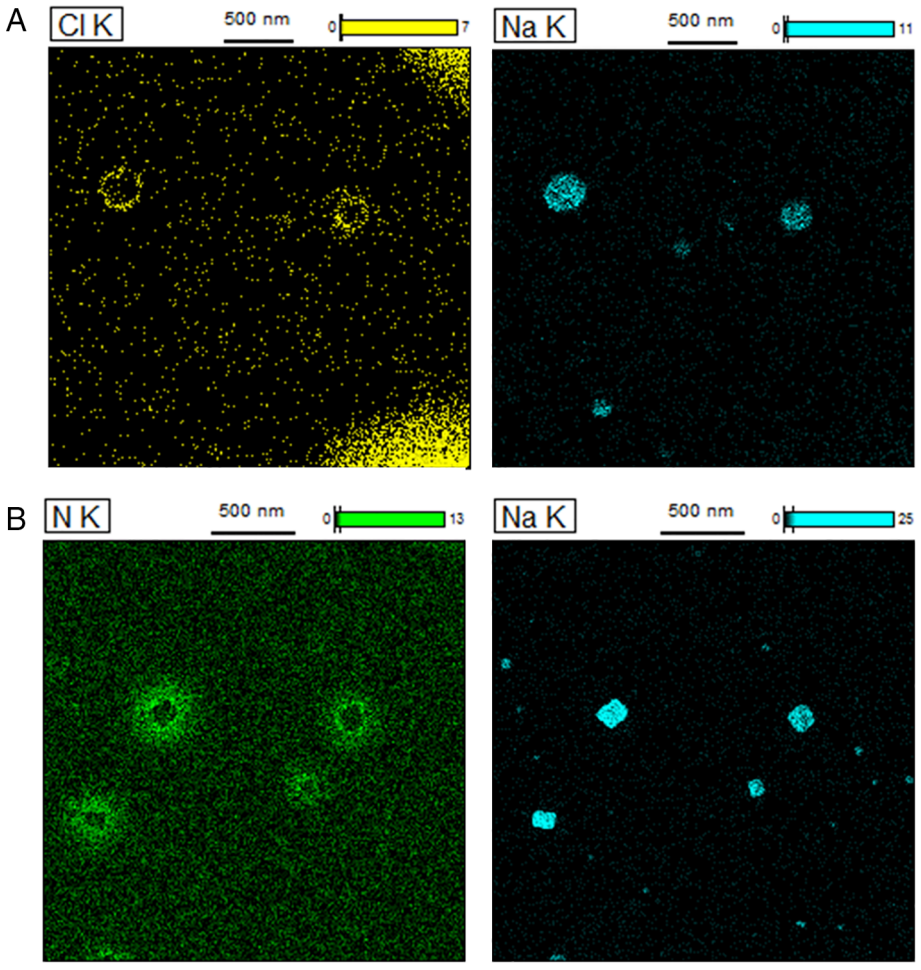

Fig. 5. TEM-EDS images of (*A*) ACM + $NaNO_2$ and (*B*) ACM + NaCl particles. The concentrations in the atomized solutions were [ACM], 4.9 mM; [$NaNO_2$], 20.9 mM; and [NaCl], 20.9 mM.

cause hydrolysis of the products was taken up into the particles. The exception to this is the peak assigned to ACM-descn (*m/z* 198) and ACM-P4 (*m/z* 243) (Fig. 8*B*) in which the cyano group has been lost from the parent ACM. Cyano compounds are known to be toxic to fish and mammals (72–74), hence the loss of the –CN group through this chemistry may decrease overall toxicity. It is noteworthy that ACM-desm, ACM-descn, ACM-P1, and ACM-P3 have also been detected in human urine as neonicotinoid metabolites (75, 76).

For top–down oxidation of ACM films on a screen, similar products were identified (Fig. 8 *C* and *D*), but with some differences in relative product yields compared to ACM-coated particles in the flow tube. The yield of Alcohol-A is much larger relative to Carbonyl-A and Carbonyl-B for the ACM film compared to the

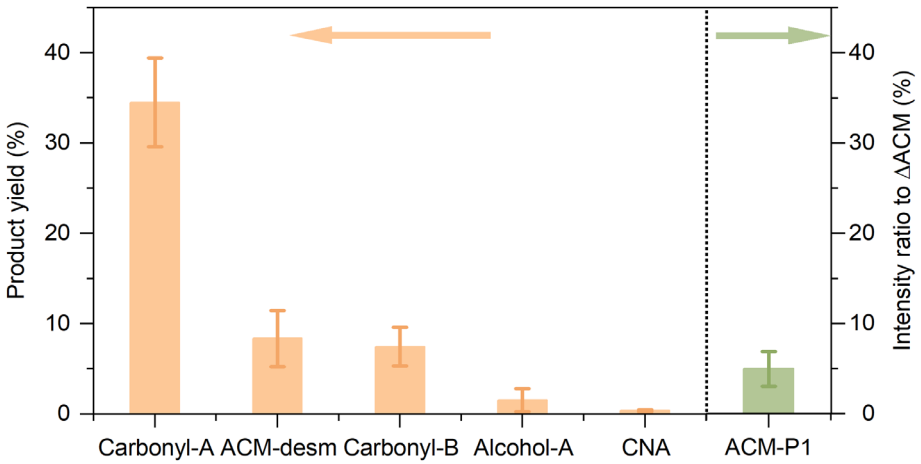

Fig. 6. Product yields (*Left* axis) and intensity ratios (*Right* axis) to the loss of ACM, ΔACM, in the OH oxidation on TiO_2, where TiO_2 photolysis in the presence of RH 50% air is the OH source.

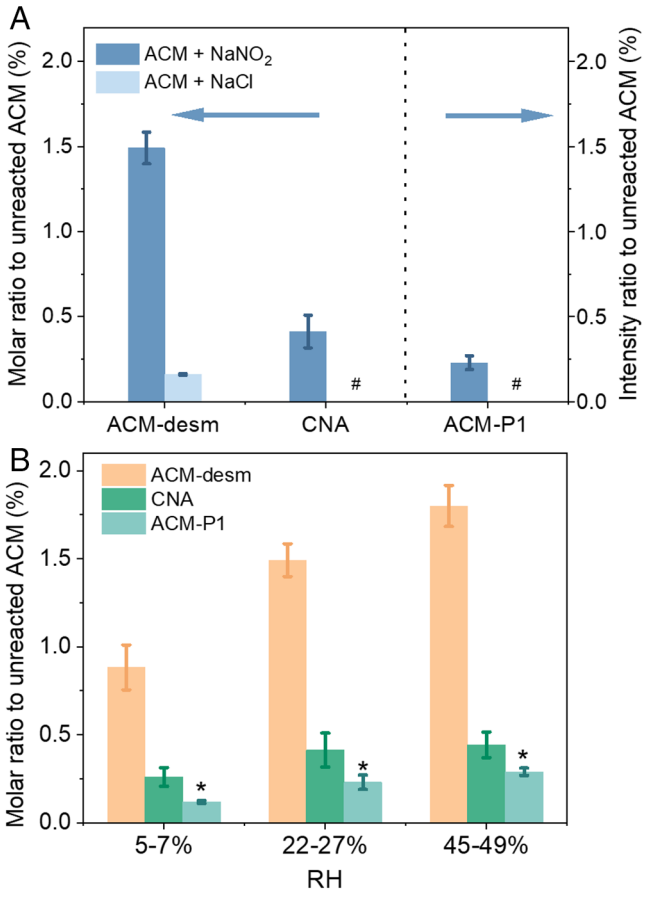

Fig. 7. (*A*) Product molar ratios (*Left* axis) and intensity ratios (*Right* axis) relative to unreacted ACM from ACM on $NaNO_2$ and NaCl particles used as a control in bottom–up experiments in AFT. Irradiation time is 15 min at RH 22 to 27%. The concentrations in the atomized solutions were [ACM], 5.5 mM; [$NaNO_2$], 15.7 mM; and [NaCl], 15.7 mM. (*B*) Molar ratios of major products to unreacted ACM in AFT experiments using $NaNO_2$ under different RH. #Not detected. *Intensity ratio to unreacted ACM.

ACM-coated NaCl particles or for the bottom–up and aqueous phase oxidations. This suggests that the RO_2 + RO_2 channel to give a carbonyl + alcohol (Fig. 4) is favored in the oxidation of the ACM film over that to give RO radicals that lead to the carbonyl products. This likely reflects higher concentrations of OH and hence RO_2 radicals generated from the higher light intensity of the xenon lamp used in the experiments on ACM films, thus favoring RO_2 + RO_2 over RO_2 + NO.

The formation of ACM-descn, ACM-P3, and ACM-P4, are attributed to addition of OH to the carbon atom of the cyano group (Fig. 9). The addition of OH to a cyano group has been observed in the reaction of acetonitrile with OH in the gas phase (77, 78). As the RH increases, the intensities of these three products, especially ACM-descn, decrease (with the possible exception of ACM-P3 for the ACM-NaCl coated particles). This may be due to water complexing to the cyano group, protecting it from attack by OH.

In short, the oxidation of ACM results in distinct product profiles depending on the oxidation method employed: top–down, bottom–up, or aqueous phase oxidation. In bottom–up oxidation using TiO_2 photolysis as the source of OH, carbonyl compounds are the major products. Conversely, when $NaNO_2$ is used as the OH source, the hydrolysis products of carbonyl and alcohol compounds dominate, likely due to the hygroscopic nature of $NaNO_2$. Top–down oxidation reveals the significance of products formed through OH addition to the cyano group, which are not observed in bottom–up or aqueous oxidations. Under aqueous conditions, hydrolysis to form ACM-desm is dominant. Although not measured here, volatile organics such as formaldehyde and formic acid are expected to be generated (Fig. 3) and easily released into the gas phase during top–down oxidation. This study underscores the diverse potential environmental fates of ACM, depending on the point of attack by OH and the availability of water.

Environmental Significance

The lifetime of ACM on surfaces in the environment will be determined by the reaction kinetics combined with the concentrations of OH radicals in the gas phase that can attack from the top–down and by the amounts of OH generated by photocatalysts that attack from the bottom–up.

Top–Down Oxidation. For top–down oxidation, the lifetimes can be estimated from the gas–solid ACM reaction probability and known atmospheric concentrations of OH. Reaction probabilities (γ) for the ACM oxidation by gas phase OH were measured by following the initial rates of loss of ACM (R_0) in a thin film on an ATR crystal (*SI Appendix*, *Text S3* and Fig. S10) as described in *Materials and Methods* below. *SI Appendix*, Tables S1 and S2 summarize R_0 and γ for the reaction of OH with ACM, and for comparison, for reactions with some other neonicotinoid nitroguanidines. The reaction probability for gas phase OH with ACM is 0.11 ± 0.03 (1σ), significantly larger than those for the OH reaction with the NN IMD, DNF, and CLD (*SI Appendix*, Table S2).

Theoretical rate constants for gas phase OH reactions were calculated based on hydrogen abstraction using SAR (42), giving values of 2.40×10^{-11}, 2.50×10^{-11}, 1.07×10^{-11}, and 1.08×10^{-11} cm^3 $molecule^{-1}$ s^{-1} for IMD, DNF, CLD, and ACM, respectively. The relative value predicted for ACM with a –CN group is smaller than those for IMD and DNF, and the same as that for CLD, all of which have a remote $–NO_2$ group. SAR calculations do not take into account such remote group effects. Although the adjacent amine nitrogen accelerates abstraction of hydrogen from a neighboring C–H bond, both –CN and $–NO_2$ are strong electron-withdrawing groups, with $–NO_2$ having a stronger electron-withdrawing power than –CN (79). This is expected to slow down the reactions, but these remote group effects are not taken into account in the SAR calculations.

An initial lifetime of ACM was calculated using an atmospherically relevant OH concentration of 10^6 radicals cm^{-3} and a surface concentration of ACM molecules of approximately 2.4×10^{14} cm^{-2} (*SI Appendix*, *Text S3*) (80). Using the experimentally measured reaction probability of 0.11 (*SI Appendix*, Table S2), the calculated lifetime predicted for ACM is about 2 d. This is a lower limit since the OH concentration will be much smaller during the dark periods of the day. However, this lifetime is much shorter than the previously reported ACM lifetimes for soil degradation, photolysis, and hydrolysis (76, 81).

Bottom–Up Oxidation. Quantifying the production of OH at the TiO_2 interface with ACM to obtain rates of bottom–up oxidation relative to the top–down process is challenging, so a different approach was taken to assess its importance relative to the top–down oxidation. Briefly, ACM and ACM on TiO_2 were exposed to sunlight outdoors in the presence of water at two locations, one at a high altitude (Fawnskin, CA, 7,000 ft) and one close to sea level (Irvine, CA). After exposure, the mixture of unreacted ACM and the reaction products were extracted and analyzed by liquid chromatography-mass spectrometry.

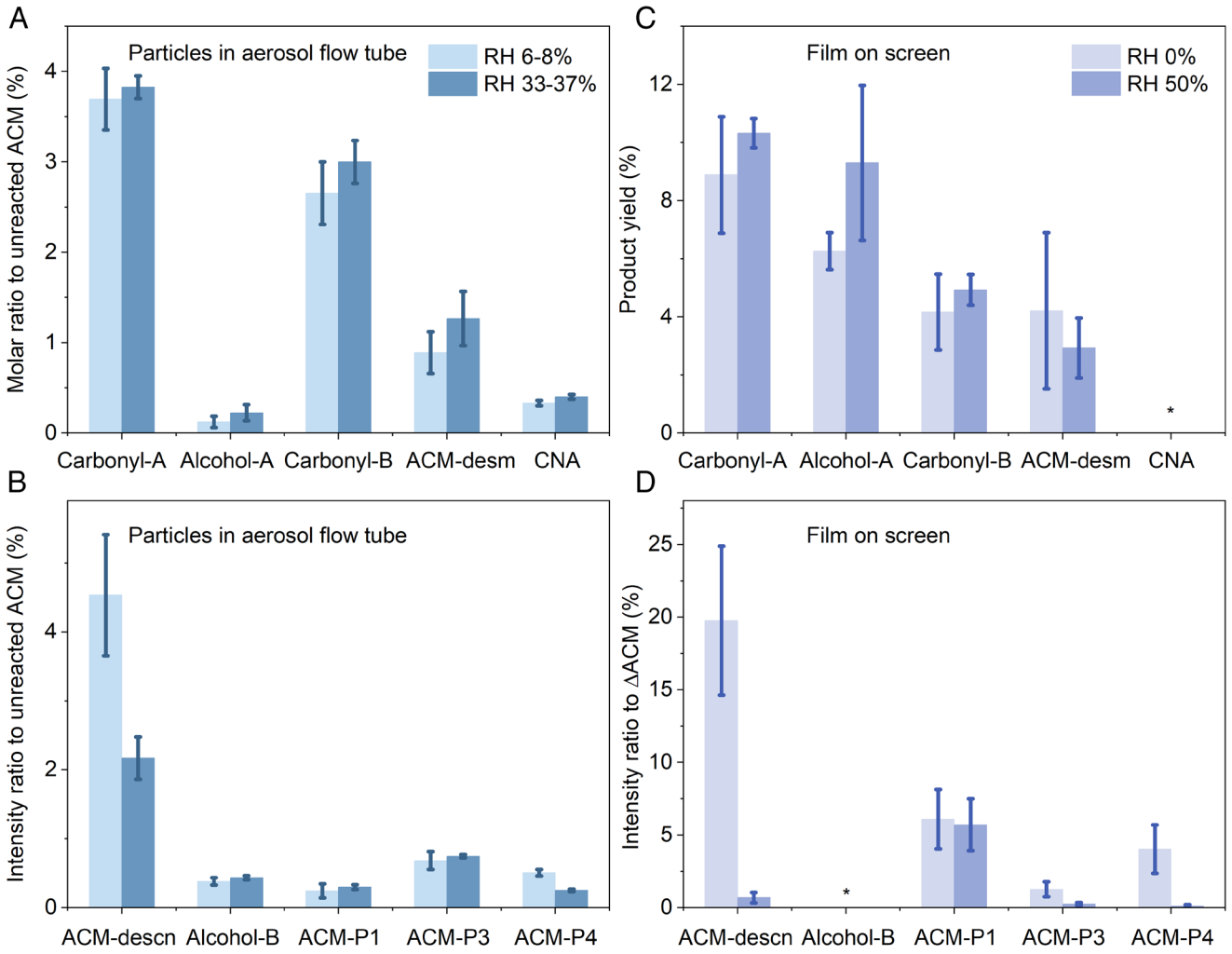

Fig. 8. (*A*) Molar and (*B*) intensity ratios of products to the unreacted ACM in AFT top–down experiment using ACM on NaCl particles under different RH. Irradiation time: 15 min; The concentrations in the atomized solutions were [ACM]: 4.9 mM; [NaCl]: 20.9 mM. The IPN concentration was ~100 ppm. (*C*) Product yields and (*D*) intensity ratios of products to the ACM loss, ΔACM, in the gas phase OH (IPN + UV) oxidation with ACM film on a screen. *Not detected.

The outdoor exposures of ACM alone (no TiO_2) showed some loss (17 to 30%), but it was significantly less than that in the presence of TiO_2 (59 to 63%). The total product yields for ACM alone were much smaller, a total of 2 to 3% compared to 27 to 35% with TiO_2, indicating that direct photolysis and reaction with OH top–down were not significant. The loss of ACM without the corresponding formation of products is likely due mainly to evaporation of ACM at the higher outdoor temperatures (above 30 °C), since the estimated vapor pressure of ACM, 4.4×10^{-5} Torr equivalent to 58 ppb, is relatively high for a NN even at 25 °C (82).

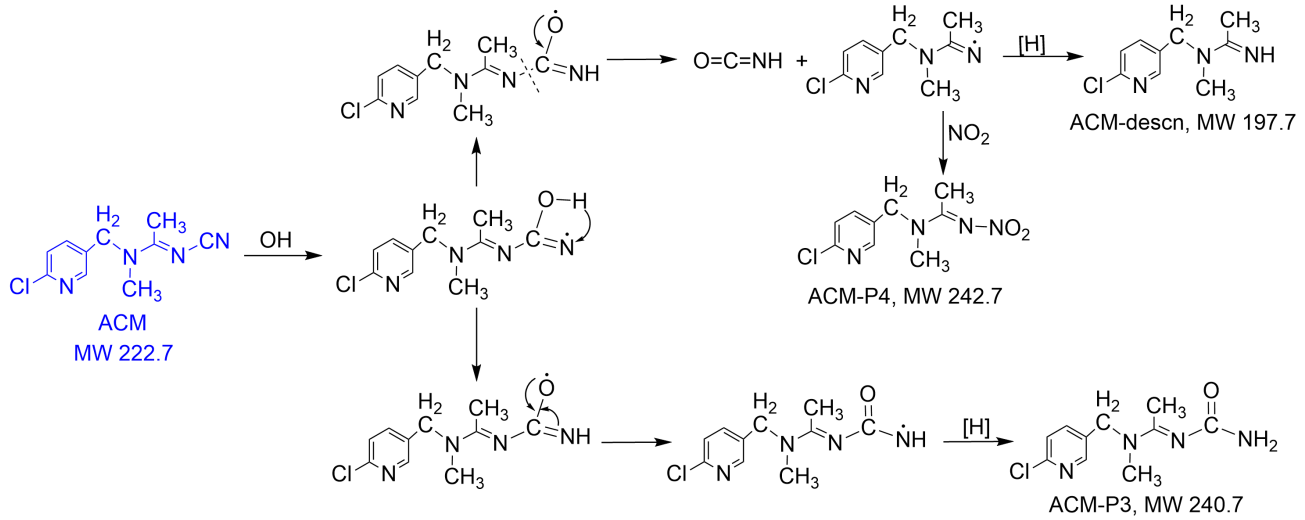

Fig. 9. Proposed mechanisms for reaction products from addition of OH to –CN group in ACM. NO_2 was generated during IPN photolysis.

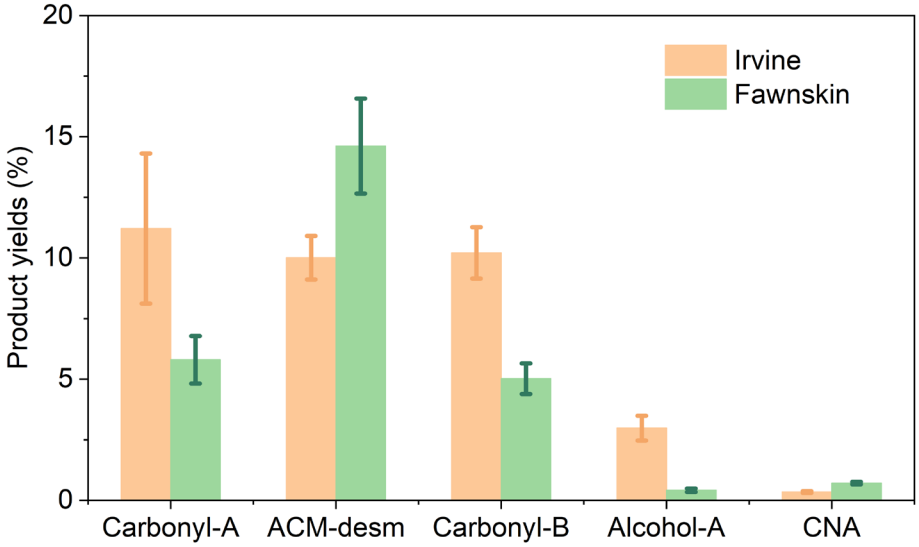

Fig. 10. Relative product yields from the exposure of ACM/TiO_2 films deposited on the screen to natural sunlight outdoors at two locations.

While quantitative kinetics could not be extracted from these experiments, the losses of ACM give an indication of the relative importance of bottom–up versus top–down processes. Taking the Irvine samples as an example, 59% of the initial ACM was lost in 11 h in the presence of TiO_2. This includes loss by evaporation which was about 17% based on the ACM alone loss, suggesting about 42% loss of ACM due to reaction on TiO_2 over 11 h. Assuming the loss is a first-order process, the first-order rate constant is ~1.4×10^{-5} s^{-1}, giving a lifetime of about 20 h. However, this is a lower limit since it is based on the loss on pure TiO_2 and would have to be scaled for the fraction of TiO_2 found on surfaces. Comparison to the estimated top–down lifetime of about 2 d suggests that losses due to both top–down and bottom–up will contribute to the degradation of ACM in the environment. The loss of ACM with only small amounts of product formation in the outdoor experiments in the absence of TiO_2 supports a long lifetime for top–down oxidation relative to bottom–up under those conditions. In any event, the degradation of ACM in the environment will predominantly occur through reaction with OH radicals, in contrast to NN nitroguanidines where photolysis is the primary environmental degradation pathway (43, 83, 84).

Fig. 10 summarizes the product yields for the ACM/TiO_2 samples at both locations. The products from the outdoor exposures follow those observed in the laboratory studies using TiO_2 (Fig. 6), but with somewhat different relative yields. For example, Carbonyl-A is the major product under laboratory conditions, while Carbonyl-A and ACM-desm have similar yields for the outdoor exposures. This likely reflects the presence of more water in the outdoor exposures, resulting in the hydrolysis of Carbonyl-A to form ACM-desm (Fig. 3). Carbonyl-A, Carbonyl-B and Alcohol-A are significantly smaller for the Fawnskin samples compared to those exposed in Irvine, and ACM-desm is larger. This is likely due to the high RH during part of the Fawnskin exposures as water condensed on the quartz covers (*Materials and Methods*).

It has been reported that ACM-desm exhibits lower toxicity compared to the parent ACM (32, 85). However, carbonyl compounds emerge as major products during ACM oxidation in top–down oxidation as well as in ACM-coated TiO_2 film experiments, with yields from 13 to 42%. These carbonyl compounds are different from previously reported metabolites in risk assessments (76). Whether they are more or less toxic than the parent compound remains to be investigated and included in the future risk assessments for ACM.

Understanding the mechanisms for top–down and bottom–up pathways and how this impacts product formation and distributions is broadly applicable to a wide variety of systems where organics are adsorbed on surfaces, such as particles, soils, and building materials. These data will provide us with a comprehensive understanding of the environmental fates of a variety of organic emerging contaminants and help in the evaluation of the influence of both the contaminants and their degradation products on the environment.

Materials and Methods

Hydroxyl Radical Sources. OH radicals were generated in three ways: in the gas phase to provide top–down oxidation, at the surface of solid substrates to provide bottom–up oxidation, and in water solutions to provide aqueous phase oxidation.

Gas phase. Gaseous OH radicals were generated from the photolysis of isopropyl nitrite (IPN, Karl Industries, Ohio) via reactions R1–R3 (43, 86):

$$(CH_3)_2CHONO + h\nu(\lambda < 450nm) \rightarrow (CH_3)_2CHO^{\bullet} + NO, \quad [\mathbf{R1}]$$

$$(CH_3)_2CHO^{\bullet} + O_2 \rightarrow CH_3C(O)CH_3 + HO_2, \quad [\mathbf{R2}]$$

$$HO_2 + NO \rightarrow OH + NO_2. \quad [\mathbf{R3}]$$

Aqueous phase. The photolysis of sodium nitrite ($NaNO_2$, Sigma-Aldrich, 99.5%) in water was chosen as a source of OH radicals (reactions R4 and R5) (64):

$$NO_2^- + h\nu(\lambda < 400nm) \rightarrow NO + O^-, \quad [\mathbf{R4}]$$

$$O^- + H_2O \rightarrow OH + OH^-. \quad [\mathbf{R5}]$$

While other OH sources such as H_2O_2 or O_3 photolysis are commonly used for aqueous phase OH generation, $NaNO_2$ was chosen here for aqueous oxidation studies to provide consistency with bottom–up studies in which solid $NaNO_2$ particles were used. For the aqueous phase oxidation, a solution of ACM (5.5 mM) and $NaNO_2$ (15.7 mM) was exposed to radiation from a low-pressure mercury lamp with organic phosphor coating (UVP, D-28865), which emitted light centered at 350 nm (*SI Appendix*, Fig. S5*A*). Control experiments were performed using separate ACM and NaCl solutions.

Surface-generated OH. Solid $NaNO_2$ particles at RH below the deliquescence point of $NaNO_2$ (67%) (65) were used to generate OH in the particles. These particles were coated with ACM so that oxidation took place at the $NaNO_2$-ACM interface.

TiO_2 was also used to generate OH at the solid TiO_2-ACM interface. Anatase (Sigma Aldrich, 99.8%) is a stable polymorph of TiO_2 and was selected due to

its high level of photocatalytic activity (46, 51–54). Upon light absorption, an electron–hole pair (h^+, e^-) is generated, which can react with O_2 or H_2O:

$$TiO_2 + h\nu\,(\lambda < 390nm) \rightarrow h^+ + e^-, \quad [\mathbf{R6}]$$

$$e^- + O_2 \rightarrow O_2^-, \quad [\mathbf{R7}]$$

$$h^+ + H_2O \rightarrow OH + H^+. \quad [\mathbf{R8}]$$

Outdoor Exposures of ACM and ACM/TiO_2. A suspension of TiO_2 in acetonitrile (ACN, Fisher Scientific, HPLC grade) was deposited onto a stainless steel screen, and ACM added on top by evaporation from an ACN solution. A similar set of screens containing only ACM was also prepared. The screens were placed over filter paper which had been soaked with water to generate OH during TiO_2 photocatalysis. For one set of samples, quartz windows were used as covers and the samples were placed outside in direct sunlight for a total of 22 h over 3 consecutive days at Fawnskin, CA, a high elevation location (7,000 ft, latitude 34° 16' 5" N; longitude: 116° 56' 33" W). A second equivalent set without covers was exposed for a total of 11 h at low elevation (Irvine, CA, 56 ft, latitude 33° 40' 10'' N; longitude: 117° 49' 23'' W). In the case of the high altitude samples, the increase in temperature during the day resulted in water condensing on the inside of the quartz covers; to avoid liquid water coming in contact with the samples, when the water droplets were observed, they were removed using a wipe. Both sets of samples were extracted with ACN and analyzed using the Waters UPLC-TQ Absolute-MS platform (*SI Appendix*, *Text S4* and Table S3).

Aerosol Flow Tube Experiments. As shown in *SI Appendix*, Fig. S4*A*, experiments were carried out at atmospheric pressure using a jacketed aerosol flow tube (7.6 cm internal diameter and 130 cm length) made of borosilicate glass (87). There were eight UV lamps (Sylvania, F15T8/350BL) surrounding the AFT with a continuous emission spectrum over 300 to 420 nm (*SI Appendix*, Fig. S5*A*). Purge air with a flow rate of 8 L min^{-1} was injected through the external jacket to cool the AFT when UV lamps were turned on.

Particles coated with ACM were generated by atomizing a solution of ACM (AK Scientific, 98%) with NaCl (Fisher Scientific, 99.8%) or with $NaNO_2$ in water (18.2 MΩ cm) with a constant-output atomizer (TSI, Model 3076) using ultrahigh purity air (Linde Gas & Equipment Inc.) at a flow rate of 1.8 L min^{-1}. The particles passed through two silica gel diffusion dryers resulting in a relative humidity (RH) of the aerosol stream of 10 to 15%. A portion of the aerosol flow (220 mL min^{-1}) was injected into AFT with pure air, humidified air, or IPN in air at a total flow rate of 400 mL min^{-1} that gave an irradiation time of 15 min. The trap containing liquid IPN was maintained at 263 K. The total air flow of IPN was 1.07 L min^{-1}, but only approximately 70 mL min^{-1} was injected into the AFT.

IPN photolysis was employed as the source of OH radicals to initiate oxidation from the top–down while using NaCl as seed particles for ACM. Nitrite ion photolysis using $NaNO_2$ served as the source of OH radicals for bottom–up oxidation.

The particle flow was further diluted with 1 L min^{-1} pure air before being sampled into a scanning mobility particle sizer (SMPS, TSI, impactor size 0.0508 cm) to obtain particle size distributions. The SMPS consists of an electrostatic classifier (model 3082), a long differential mobility analyzer (model 3081), and a condensation particle counter (model 3756). The aerosol flow was passed through a carbon denuder and the particles were collected on a Teflon filter (Fluoropore™ Membrane Filters, PTFE, 0.2 μm) with the aid of a pump for offline analysis.

After sample collection, filters were immediately cut into pieces and extracted with 3 mL ACN using a Vortex Mixer for 15 min. The extracts were analyzed using an LC–MS equipped with a high-resolution Orbitrap mass spectrometer with heated electrospray ionization (HESI-Orbitrap HRMS, Thermo Scientific, Q Exactive Plus) for product identification. For quantification, samples were analyzed using an LC–MS equipped with a triple quadrupole mass analyzer (UPLC-TQD-MS, Waters) in the multiple reaction monitoring (MRM) mode. The MRM transitions for ACM and its oxidation products are shown in *SI Appendix*, Table S3. More details about these analytical platforms can be found elsewhere (88) and in *SI Appendix*, *Text S4*.

Authentic samples of *N*-(6-chloro-3-pyridylmethyl)-*N'*-cyano-acetamidine (ACM-desm, LGC standards, 100 μg mL^{-1} in ACN, 98.4%) and 6-chloronicotinic acid (CNA, Fisher scientific, 99%) were used for product identification and quantification.

Morphology of ACM/NaCl/$NaNO_2$/TiO_2 Particles and Films. A typical size distribution of ACM-coated NaCl or $NaNO_2$ is shown in *SI Appendix*, Fig. S11, where the mode diameter is seen to be ~120 nm. The morphologies and elemental composition of films and individual particles were determined by using a scanning transmission electron microscope (TEM, JEOL JEM-2800, USA) with energy dispersive X-ray spectroscopy (EDS). More details on the TEM-EDS analysis are given in *SI Appendix*, *Text S5*.

ACM Film Experiments.

Kinetic studies. Kinetics studies of gaseous OH oxidation of ACM film from the top–down were carried out by attenuated total reflectance Fourier transform infrared spectrometry (ATR-FTIR, Mattson Galaxy 5020) as in our previous studies of neonicotinoid nitroguanidines (*SI Appendix*, Fig. S4*B*) (43, 89). Briefly, a small amount of ACM in ACN solution was pipetted onto the surface of a ZnSe ATR crystal [80 mm (l) × 10 mm (w) × 4 mm (d), 45° entrance angle, 10 internal reflections, Pike Technologies] and an amorphous thin film of ACM was formed during the fast evaporation of ACN (67, 68). The initial amount of deposited ACM was in the range of 7.8×10^{15} to 1.6×10^{17} molecules. Assuming that ACM molecules were evenly dispersed in the film, the number of ACM monolayers was calculated to be 8 to 167 using a unit cell volume of 1,100.49 $Å^3$ for ACM with 4 molecules per unit cell (80) and 4 cm^2 of ATR probing surface area. The maximum ACM film thickness of 0.11 μm was less than the depth of IR penetration of 0.53 μm at the -CN absorption at 2,173 cm^{-1} (90), thus the entire film was probed by ATR-FTIR.

For top–down oxidation, pure oxygen (Praxair, 99.993%) at a flow rate of 500 mL min^{-1} either flowed directly or passed over the headspace of a trap containing liquid IPN held at 263 K into the custom reaction cell (*SI Appendix*, Fig. S4*B*). A high-pressure Xe lamp (Ushio 300 W bulb, UXL-302-O) equipped with a power source (Newport model 69911) was used to photolyze the IPN/O_2 flow in the cell. A quartz water filter and an optical filter (Newport longpass colored glass alternative filter, 20CGA-360) were used to remove infrared irradiation and light below 360 nm, respectively.

The loss of ACM due to its reaction with OH and the formation of products were monitored using ATR-FTIR with 32 coadded scans at a resolution of 4 cm^{-1}. FTIR spectra were recorded before and during irradiation while IPN/O_2 continuously flowed over the ACM film. A calibration curve correlating ACM concentration to FTIR absorbance was established by depositing known amounts of ACM on the ATR crystal.

Product studies. Product studies of the ACM reaction with OH were carried out in a 60 cm^3 glass cell, either with IPN or TiO_2 as the OH precursor (*SI Appendix*, Fig. S4*C*). A known amount of ACM in ACN (~10 μL of 1 mg mL^{-1} solution) was first deposited on a stainless-steel screen (McMaster-Carr, SST 304, 74 mesh, 0.0037" DIA, 53% open area). ACN was evaporated rapidly and the ACM coated screen was then placed inside the glass reaction cell. The initial amount of ACM on 1 cm^2 of the mesh was ~6×10^{16} molecules, corresponding to ~250 monolayers. The cell was irradiated using a high-pressure Xe lamp with a water filter while flowing IPN/air through the cell for top–down oxidation. When using TiO_2 as OH source for bottom–up oxidation, TiO_2 was sonicated in ACN for at least 15 min, generating a colloidal suspension (~3.75 mg mL^{-1}) which was deposited on the stainless steel screen (~20 μL per 1 cm^2). After ACN evaporated, an ACM solution (~10 μL of 1 mg mL^{-1} solution) was deposited on top of TiO_2 and the solvent evaporated. While the TiO_2 particle size was not measured, diameters between 0.1 and 1 μm are reasonable. In this case, the total number of effective monolayers is ~10 to 100 layers. The ACM/TiO_2 mixture on the screen was photolyzed in the cell while flowing humid air at RH 50%. After UV irradiation, ACM and its oxidation products were extracted with ACN for LC–MS analysis (*SI Appendix*, *Text S4*).

Data, Materials, and Software Availability. All study data are included in the article and/or *SI Appendix*.

ACKNOWLEDGMENTS. We are grateful to the NSF for support (grants #2303948 and 2002909 and equipment grants #1920242 and 1337080) and the Army Research Office for an equipment grant (#W911NF2010064). We thank Dr. Mingjie Xu for the help of (Cryo-)TEM-EDS analysis and acknowledge the use of facilities and instrumentation at the UC Irvine Materials Research Institute (IMRI), which is supported in part by the NSF through the UC Irvine Materials Research Science and Engineering Center (DMR-2011967). We also thank the UCI Mass Spectrometry Facility and Dr. Felix Grun and Dr. Benjamin Katz for assistance with method development and quantitative LC–MS/MS analysis of ACM and its oxidation products from the outdoor exposures. Data were collected on a Waters Acquity UPLC and TQ Absolute Premier triple quadrupole system for which funding support was provided by UCI's Office of Research, MS Facility, and the Schools of Physical Sciences/Engineering/Biological Sciences/Medicine and Pharmacology & Pharmaceutical Sciences.

1. P. Jeschke, R. Nauen, M. Schindler, A. Elbert, Overview of the status and global strategy for neonicotinoids. *J. Agric. Food Chem.* **59**, 2897–2908 (2011).
2. J. M. Bonmatin *et al.*, Environmental fate and exposure; neonicotinoids and fipronil. *Environ. Sci. Pollut. Res.* **22**, 35–67 (2015).
3. E. A. D. Mitchell *et al.*, A worldwide survey of neonicotinoids in honey. *Science* **358**, 109–111 (2017).
4. K. A. Stoner, B. D. Eitzer, Movement of soil-applied imidacloprid and thiamethoxam into nectar and pollen of squash (Cucurbita pepo). *PLoS One* **7**, 1–5 (2012).
5. T. J. Wood, D. Goulson, The environmental risks of neonicotinoid pesticides: A review of the evidence post 2013. *Environ. Sci. Pollut. Res.* **24**, 17285–17325 (2017).
6. A. Tapparo *et al.*, Assessment of the environmental exposure of honeybees to particulate matter containing neonicotinoid insecticides coming from corn coated seeds. *Environ. Sci. Technol.* **46**, 2592–2599 (2012).
7. A. Voloshenko Rossin, S. Sladkevich, G. Gasser, A. Melman, O. Lev, Sensitive analysis of nitroguanidine in aqueous and soil matrices by LC-MS. *Anal. Chem.* **89**, 9990–9996 (2017).
8. M. Chen, L. Tao, J. McLean, C. Lu, Quantitative analysis of neonicotinoid insecticide residues in foods: Implication for dietary exposures. *J. Agric. Food Chem.* **62**, 6082–6090 (2014).
9. H. Obana, M. Okihashi, K. Akutsu, Y. Kitagawa, S. Hori, Determination of acetamiprid, imidacloprid, and nitenpyram residues in vegetables and fruits by high-performance liquid chromatography with diode-array detection. *J. Agric. Food Chem.* **50**, 4464–4467 (2002).
10. K. L. Klarich *et al.*, Occurrence of neonicotinoid insecticides in finished drinking water and fate during drinking water treatment. *Environ. Sci. Technol. Lett.* **4**, 168–173 (2017).
11. T. Yamamuro, H. Ohta, M. Aoyama, D. Watanabe, Simultaneous determination of neonicotinoid insecticides in human serum and urine using diatomaceous earth-assisted extraction and liquid chromatography-tandem mass spectrometry. *J. Chromatogr. B Anal. Technol. Biomed. Life Sci.* **969**, 85–94 (2014).
12. L. Wang *et al.*, Occurrence and profile characteristics of the pesticide imidacloprid, preservative parabens, and their metabolites in human urine from rural and urban China. *Environ. Sci. Technol.* **49**, 14633–14640 (2015).
13. D. Goulson, E. Nicholls, C. Botías, E. L. Rotheray, Bee declines driven by combined Stress from parasites, pesticides, and lack of flowers. *Science* **347**, 1255957 (2015).
14. M. Rundlöf *et al.*, Seed coating with a neonicotinoid insecticide negatively affects wild bees. *Nature* **521**, 77–80 (2015).
15. S. Kurwadkar, A. Evans, Neonicotinoids: Systemic insecticides and systematic failure. *Bull. Environ. Contam. Toxicol.* **97**, 745–748 (2016).
16. D. Goulson, An overview of the environmental risks posed by neonicotinoid insecticides. *J. Appl. Ecol.* **50**, 977–987 (2013).
17. L. W. Pisa *et al.*, Effects of neonicotinoids and fipronil on non-target invertebrates. *Environ. Sci. Pollut. Res.* **22**, 68–102 (2014).
18. M. B. van Lexmond, J. M. Bonmatin, D. Goulson, D. A. Noome, Worldwide integrated assessment on systemic pesticides global collapse of the entomofauna: Exploring the role of systemic insecticides. *Environ. Sci. Pollut. Res.* **22**, 1–4 (2015).
19. U. Černigoj, U. L. Štangar, P. Trebše, Degradation of neonicotinoid insecticides by different advanced oxidation processes and studying the effect of ozone on TiO_2 photocatalysis. *Appl. Catal. B Environ.* **75**, 229–238 (2007).
20. S. Kanan, M. Moyet, K. Obeideen, Y. El-Sayed, A. A. Mohamed, *Occurrence, Analysis and Removal of Pesticides, Hormones, Pharmaceuticals, and Other Contaminants in Soil and Water Streams for the Past Two Decades: A Review* (Springer, Netherlands, 2022).
21. C. Giorio *et al.*, An update of the Worldwide Integrated Assessment (WIA) on systemic insecticides. Part 1: New molecules, metabolism, fate, and transport. *Environ. Sci. Pollut. Res.* **28**, 11716–11748 (2021).
22. Y. Li, Y. Li, G. Bi, T. J. Ward, L. Li, Adsorption and degradation of neonicotinoid insecticides in agricultural soils. *Environ. Sci. Pollut. Res.* **30**, 47516–47526 (2023).
23. J. Fenoll, I. Garrido, P. Hellín, P. Flores, S. Navarro, Photodegradation of neonicotinoid insecticides in water by semiconductor oxides. *Environ. Sci. Pollut. Res.* **22**, 15055–15066 (2015).
24. V. Kosar, F. Kurt, V. Tomašić, I. E. Zelić, Analysis and modelling of photodegradation of neonicotinoid insecticides under the influence of UVA-LED radiation. *React. Kinet. Mech. Catal.* **134**, 989–1001 (2021).
25. F. Karagulian, C. W. Dilbeck, B. J. Finlayson-Pitts, Unusual oxidation of organics at interfaces from the bottom up and atmospheric implications. *J. Am. Chem. Soc.* **130**, 11272–11273 (2008).
26. J. P. Reid *et al.*, The morphology of aerosol particles consisting of hydrophobic and hydrophilic phases: Hydrocarbons, alcohols and fatty acids as the hydrophobic component. *Phys. Chem. Chem. Phys.* **13**, 15559–15572 (2011).
27. M. Song, C. Marcolli, U. K. Krieger, D. M. Lienhard, T. Peter, Morphologies of mixed organic/inorganic/aqueous aerosol droplets. *Faraday Discuss.* **165**, 289–316 (2013).
28. D. P. Veghte, D. R. Bittner, M. A. Freedman, Cryo-transmission electron microscopy imaging of the morphology of submicrometer aerosol containing organic acids and ammonium sulfate. *Anal. Chem.* **86**, 2436–2442 (2014).
29. K. Gorkowski, N. M. Donahue, R. C. Sullivan, Aerosol optical tweezers constrain the morphology evolution of liquid-liquid phase-separated atmospheric particles. *Chem* **6**, 204–220 (2020).
30. T. M. Kucinski, J. N. Dawson, M. A. Freedman, Size-dependent liquid-liquid phase separation in atmospherically relevant complex systems. *J. Phys. Chem. Lett.* **10**, 6915–6920 (2019).
31. Y. Huang *et al.*, Coexistence of three liquid phases in individual atmospheric aerosol particles. *Proc. Natl. Acad. Sci. U.S.A.* **118**, e2102512118 (2021).
32. M. L. Dell'Arciprete *et al.*, Reactivity of hydroxyl radicals with neonicotinoid insecticides: Mechanism and changes in toxicity. *Photochem. Photobiol. Sci.* **8**, 1016–1023 (2009).
33. I. Carra *et al.*, Degradation and monitoring of acetamiprid, thiabendazole and their transformation products in an agro-food industry effluent during solar photo-Fenton treatment in a raceway pond reactor. *Chemosphere* **130**, 73–81 (2015).
34. I. Carra *et al.*, Application of high intensity UVC-LED for the removal of acetamiprid with the photo-Fenton process. *Chem. Eng. J.* **264**, 690–696 (2015).
35. V. J. Guzsvány, J. J. Csanádi, S. D. Lazić, F. F. Gaál, Photocatalytic degradation of the insecticide acetamiprid on TiO_2 Catalyst. *J. Braz. Chem. Soc.* **20**, 152–159 (2009).
36. I. E. Zelić, K. Povijač, V. Gilja, V. Tomašić, Z. Gomzi, Photocatalytic degradation of acetamiprid in a rotating photoreactor – Determination of reactive species. *Catal. Commun.* **169**, 1–7 (2022).
37. K. Licht, V. Kosar, V. Tomašić, M. Duplančić, Removal of the neonicotinoid insecticide acetamiprid from wastewater using heterogeneous photocatalysis. *Environ. Technol.* **44**, 1125–1134 (2023).
38. A. Cruz-Alcalde, C. Sans, S. Esplugas, Priority pesticides abatement by advanced water technologies: The case of acetamiprid removal by ozonation. *Sci. Total Environ.* **599–600**, 1454–1461 (2017).
39. G. Xie, G. Liu, D. Sun, L. Zheng, Kinetics of acetamiprid photolysis in solution. *Bull. Environ. Contam. Toxicol.* **82**, 129–132 (2009).
40. L. Chen, T. Cai, C. Cheng, Z. Xiong, D. Ding, Degradation of acetamiprid in UV/H_2O_2 and UV/persulfate systems: A comparative study. *Chem. Eng. J.* **351**, 1137–1146 (2018).
41. B. J. Finlayson-Pitts, J. N. Pitts, *Chemistry of the Upper and Lower Atmosphere: Theory, Experiments, and Applications* (Academic Press, 2000).
42. E. Kwok, R. Atkinson, Estimation of hydroxyl radical reaction rate constants for gas-phase organic compounds using a structure-reactivity relationship: An update. *Atmos. Environ.* **29**, 1685–1695 (1995).
43. B. J. Finlayson-Pitts *et al.*, Oxidation of solid thin films of neonicotinoid pesticides by gas phase hydroxyl radicals. *Environ. Sci. Atmos.* **3**, 124–142 (2023).
44. D. D. M. Wayner, K. B. Clark, A. Rauk, D. Yu, D. A. Armstrong, C–H bond dissociation energies of alkyl amines: Radical structures and stabilization energies. *J. Am. Chem. Soc.* **119**, 8925–8932 (1997).
45. T. J. Burkey, A. L. Castelhano, D. Griller, F. P. Lossing, Heats of formation and ionization potentials of some α-aminoalkyl radicals. *J. Am. Chem. Soc.* **105**, 4701–4703 (1983).
46. H. Chen, C. E. Nanayakkara, V. H. Grassian, Titanium dioxide photocatalysis in atmospheric chemistry. *Chem. Rev.* **112**, 5919–5948 (2012).
47. A. Fujishima, X. Zhang, D. A. Tryk, TiO_2 photocatalysis and related surface phenomena. *Surf. Sci. Rep.* **63**, 515–582 (2008).
48. I. P. Parkin, R. G. Palgrave, Self-cleaning coatings. *J. Mater. Chem.* **15**, 1689–1695 (2005).
49. M. M. Ballari, Q. L. Yu, H. J. H. Brouwers, Experimental study of the NO and NO_2 degradation by photocatalytically active concrete. *Catal. Today* **161**, 175–180 (2011).
50. M. M. Ballari, M. Hunger, G. Hüsken, H. J. H. Brouwers, NO_x photocatalytic degradation employing concrete pavement containing titanium dioxide. *Appl. Catal. B Environ.* **95**, 245–254 (2010).
51. Q. Guo, C. Zhou, Z. Ma, X. Yang, Fundamentals of TiO_2 photocatalysis: Concepts, mechanisms, and challenges. *Adv. Mater.* **31**, 1–26 (2019).
52. A. L. Linsebigler, G. Lu, J. T. Yates, Photocatalysis on TiO_2 surfaces: Principles, mechanisms, and selected results. *Chem. Rev.* **95**, 735–758 (1995).
53. M. A. Henderson, A surface science perspective on TiO_2 photocatalysis. *Surf. Sci. Rep.* **66**, 185–297 (2011).
54. M. A. Henderson, N. A. Deskins, R. T. Zehr, M. Dupuis, Generation of organic radicals during photocatalytic reactions on TiO_2. *J. Catal.* **279**, 205–212 (2011).
55. S. Malato, P. Fernández-Ibáñez, M. I. Maldonado, J. Blanco, W. Gernjak, Decontamination and disinfection of water by solar photocatalysis: Recent overview and trends. *Catal. Today* **147**, 1–59 (2009).
56. M. R. Hoffmann, S. T. Martin, W. Choi, D. W. Bahnemann, Environmental applications of semiconductor Photocatalysis. *Chem. Rev.* **95**, 69–96 (1995).
57. M. Ndour, M. Nicolas, B. D'Anna, O. Ka, C. George, Photoreactivity of NO_2 on mineral dusts originating from different locations of the Sahara desert. *Phys. Chem. Chem. Phys.* **11**, 1312–1319 (2009).
58. M. Ndour *et al.*, Photoenhanced uptake of NO_2 on mineral dust: Laboratory experiments and model simulations. *Geophys. Res. Lett.* **35**, 1–5 (2008).
59. D. Vione, V. Maurino, C. Minero, E. Pelizzetti, Reactions induced in natural waters by irradiation of nitrate and nitrite ions. *Environ. Photochem. Part II* **2**, 221–253 (2005).
60. X. Wang *et al.*, Snowmelt leads to seasonal nitrous acid formation across northwestern China. *Geophys. Res. Lett.* **49**, e2022GL098035 (2022).
61. H. Su *et al.*, Soil nitrite as a source of atmospheric HONO and OH radicals. *Science* **333**, 1616–1618 (2011).
62. M. A. Donaldson, D. L. Bish, J. D. Raff, Soil surface acidity plays a determining role in the atmospheric-terrestrial exchange of nitrous acid. *Proc. Natl. Acad. Sci. U.S.A.* **111**, 18472–18477 (2014).
63. P. K. Simon, P. K. Dasgupta, Continuous automated measurement of gaseous nitrous and nitric acids and particulate nitrite and nitrate. *Environ. Sci. Technol.* **29**, 1534–1541 (1995).
64. J. Mack, J. R. Bolton, Photochemistry of nitrite and nitrate in aqueous solution: A review. *J. Photochem. Photobiol. A Chem.* **128**, 1–13 (1999).
65. S. Seng *et al.*, Deliquescence behavior of photo-irradiated single $NaNO_3$ droplets. *Atmos. Environ.* **183**, 33–39 (2018).
66. T. Talreja-Muthreja, K. Linnow, D. Enke, M. Steiger, Deliquescence of NaCl confined in nanoporous silica. *Langmuir* **38**, 10963–10974 (2022).
67. L. Yu, Amorphous pharmaceutical solids: Preparation, characterization and stabilization. *Adv. Drug Deliv. Rev.* **48**, 27–42 (2001).
68. A. Nakayama, M. Sukekawa, Y. Eguchi, Stereochemistry and active conformation of a novel insecticide, acetamiprid. *Pestic. Sci.* **51**, 157–164 (1997).
69. J. J. Orlando, G. S. Tyndall, Laboratory studies of organic peroxy radical chemistry: An overview with emphasis on recent issues of atmospheric significance. *Chem. Soc. Rev.* **41**, 6294–6317 (2012).
70. L. Pokorny, I. Maturana, W. H. Bortle, "Sodium nitrate and nitrite" in *Kirk-Othmer Encyclopedia of Chemical Technology*, J. I. Kroschwitz, A. Seidel, Eds. (John Wiley & Sons, 2006).
71. C. Kidd, V. Perraud, L. M. Wingen, B. J. Finlayson-Pitts, Integrating phase and composition of secondary organic aerosol from the ozonolysis of α-pinene. *Proc. Natl. Acad. Sci. U.S.A.* **111**, 7552–7557 (2014).
72. R. L. Lipnick, Outliers: Their origin and use in the classification of molecular mechanisms of toxicity. *Sci. Total Environ.* **109–110**, 131–153 (1991).
73. F. R. Johannsen, G. J. Levinskas, P. E. Berteau, D. E. Rodwell, Evaluation of the teratogenic potential of three aliphatic nitriles in the rat. *Toxicol. Sci.* **7**, 33–40 (1986).
74. R. Bhattacharya, R. M. Satpute, J. Hariharakrishnan, H. Tripathi, P. B. Saxena, Acute toxicity of some synthetic cyanogens in rats and their response to oral treatment with alpha-ketoglutarate. *Food Chem. Toxicol.* **47**, 2314–2320 (2009).
75. K. Taira, K. Fujioka, Y. Aoyama, Qualitative profiling and quantification of neonicotinoid metabolites in human urine by liquid chromatography coupled with mass spectrometry. *PLoS One* **8**, 1–12 (2013).
76. European Food Safety Authority, Peer review of the pesticide risk assessment of the active substance acetamiprid. *EFSA J.* **14**, e04610 (2016).
77. A. Galano, Mechanism of OH radical reactions with HCN and CH_3CN: OH regeneration in the presence of O_2. *J. Phys. Chem. A* **111**, 5086–5091 (2007).

78. A. J. Hynes, P. H. Wine, Kinetics and mechanism of the reaction of hydroxyl radicals with acetonitrile under atmospheric conditions. *J. Phys. Chem.* **95**, 1232–1240 (1991).
79. C. Hansch, A. Leo, R. W. Taft, A survey of Hammett substituent constants and resonance and field parameters. *Chem. Rev.* **91**, 165–195 (1991).
80. D. Chopra, T. P. Mohan, K. S. Rao, T. N. G. Row, (*E*)-N^1-[(6-Chloropyridin-3-yl)methyl]-N^2-cyano-N^1-methylacetamidine. *Acta Crystallogr. Sect. E Struct. Rep. Online* **60**, 2374–2375 (2004).
81. S. Gupta, V. T. Gajbhiye, R. K. Gupta, Effect of light on the degradation of two neonicotinoids viz acetamiprid and thiacloprid in soil. *Bull. Environ. Contam. Toxicol.* **81**, 185–189 (2008).
82. S. Kim *et al.*, PubChem 2023 update. *Nucleic Acids Res.* **51**, D1373–D1380 (2023).
83. K. Z. Aregahegn, D. Shemesh, R. B. Gerber, B. J. Finlayson-Pitts, Photochemistry of thin solid films of the neonicotinoid imidacloprid on surfaces. *Environ. Sci. Technol.* **51**, 2660–2668 (2017).
84. K. Z. Aregahegn, M. J. Ezell, B. J. Finlayson-Pitts, Photochemistry of solid films of the neonicotinoid nitenpyram. *Environ. Sci. Technol.* **52**, 2760–2767 (2018).
85. T. Chen, Y. J. Dai, J. F. Ding, S. Yuan, J. P. Ni, *N*-demethylation of neonicotinoid insecticide acetamiprid by bacterium Stenotrophomonas maltophilia CGMCC 1.1788. *Biodegradation* **19**, 651–658 (2008).
86. J. D. Raff, B. J. Finlayson-Pitts, Hydroxyl radical quantum yields from isopropyl nitrite photolysis in air. *Environ. Sci. Technol.* **44**, 8150–8155 (2010).
87. M. J. Ezell, H. Chen, K. D. Arquero, B. J. Finlayson-Pitts, Aerosol fast flow reactor for laboratory studies of new particle formation. *J. Aerosol Sci.* **78**, 30–40 (2014).
88. X. Wang *et al.*, Predicting the environmental fates of emerging contaminants: Synergistic effects in ozone reactions of nitrogen-containing alkenes. *Sci. Adv.* **9**, 1–14 (2023).
89. W. Wang *et al.*, Gas phase and gas–solid interface ozonolysis of nitrogen containing alkenes: Nitroalkenes, enamines, and nitroenamines. *J. Phys. Chem. A* **126**, 5398–5406 (2022).
90. N. J. Harrick, *Internal Reflection Spectroscopy* (Harrick Scientific Corporation, 1987).